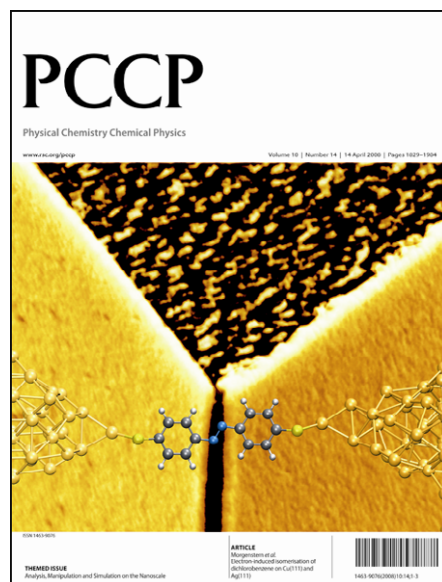


# PCCP

Physical Chemistry Chemical Physics



This article is part of a PCCP themed issue on:

[Analysis, manipulation, and simulation on the nanoscale](#)

Guest Editors: Harald Fuchs, Dominik Marx and Ulrich Simon

Other papers in the issue:

**Textile electrodes as substrates for the electrodeposition of porous ZnO**

T. Loewenstein, A. Hastall, M. Mingeback, Y. Zimmermann, A. Neudeck and D. Schlettwein, *Phys. Chem. Chem. Phys.*, 2008, **10**, 1844 (DOI: [10.1039/b719691a](#))

**Fluorescence resonance energy transfer in conjugated polymer composites for radiation detection**

Y. S. Zhao, H. Zhong and Q. Pei, *Phys. Chem. Chem. Phys.*, 2008, **10**, 1848 (DOI: [10.1039/b801375f](#))

**Simulating charge transport in tris(8-hydroxyquinoline) aluminium (Alq<sub>3</sub>)**

J. J. Kwiatkowski, J. Nelson, H. Li, J. L. Bredas, W. Wenzel and C. Lennartz, *Phys. Chem. Chem. Phys.*, 2008, **10**, 1852 (DOI: [10.1039/b719592c](#))

**Functional molecular wires**

G. J. Ashwell, P. Wierchowicz, L. J. Phillips, C. J. Collins, J. Gigon, B. J. Robinson, C. M. Finch, I. R. Grace, C. J. Lambert, P. D. Buckle, K. Ford, B. J. Wood and I. R. Gentle, *Phys. Chem. Chem. Phys.*, 2008, **10**, 1859 (DOI: [10.1039/b719417j](#))

**Forced imbibition—a tool for separate determination of Laplace pressure and drag force in capillary filling experiments**

D. I. Dimitrov, A. Milchev and K. Binder, *Phys. Chem. Chem. Phys.*, 2008, **10**, 1867 (DOI: [10.1039/b719248g](#))

**Assembly of DNA-functionalized gold nanoparticles studied by UV/Vis-spectroscopy and dynamic light scattering**

K. G. Witten, J. C. Bretschneider, T. Eckert, W. Richtering and U. Simon, *Phys. Chem. Chem. Phys.*, 2008, **10**, 1870, (DOI: [10.1039/b719762d](#))

**Metal adsorption on oxide polar ultrathin films**

G. Barcaro, A. Fortunelli and G. Granozzi, *Phys. Chem. Chem. Phys.*, 2008, **10**, 1876 (DOI: [10.1039/b719346g](#))

**Microstructure analysis of monodisperse ferrofluid monolayers: theory and simulation**

S. Kantorovich, J. J. Cerdà and C. Holm, *Phys. Chem. Chem. Phys.*, 2008, **10**, 1883 (DOI: [10.1039/b719460a](#))

**Molecular simulation study of temperature effect on ionic hydration in carbon nanotubes**

Q. Shao, L. Huang, J. Zhou, L. Lu, L. Zhang, X. Lu, S. Jiang, K. E. Gubbins and W. Shen, *Phys. Chem. Chem. Phys.*, 2008, **10**, 1896 (DOI: [10.1039/b719033f](#))

**Adsorption of small organic molecules on anatase and rutile surfaces: a theoretical study**

S. Köppen and W. Langel, *Phys. Chem. Chem. Phys.*, 2008, **10**, 1907 (DOI: [10.1039/b719098k](#))

**Electron-induced isomerisation of dichlorobenzene on Cu(111) and Ag(111)**

V. Simic-Milosevic, J. Meyer and K. Morgenstern, *Phys. Chem. Chem. Phys.*, 2008, **10**, 1916 (DOI: [10.1039/b718847a](#))

**Au–Pd supported nanocrystals prepared by a sol immobilisation technique as catalysts for selective chemical synthesis**

J. A. Lopez-Sanchez, N. Dimitratos, P. Miedziak, E. Ntainjua, J. K. Edwards, D. Morgan, A. F. Carley, R. Tiruvalam, C. J. Kiely and G. J. Hutchings, *Phys. Chem. Chem. Phys.*, 2008, **10**, 1921 (DOI: [10.1039/b719345a](#))

**Transport effects in the oxygen reduction reaction on nanostructured, planar glassy carbon supported Pt/GC model electrodes**

A. Schneider, L. Colmenares, Y. E. Seidel, Z. Jusys, B. Wickman, B. Kasemo and R. J. Behm, *Phys. Chem. Chem. Phys.*, 2008, **10**, 1931 (DOI: [10.1039/b719775f](#))

**Structure, optical properties and defects in nitride (III–V) nanoscale cage clusters**

S. A. Shevlin, Z. X. Guo, H. J. J. van Dam, P. Sherwood, C. R. A. Catlow, A. A. Sokol and S. M. Woodley, *Phys. Chem. Chem. Phys.*, 2008, **10**, 1944 (DOI: [10.1039/b719838h](#))

**Adsorption of oxalate on rutile particles in aqueous solutions: a spectroscopic, electron-microscopic and theoretical study**

C. B. Mendive, T. Bredow, A. Feldhoff, M. Blesa and D. Bahnemann, *Phys. Chem. Chem. Phys.*, 2008, **10**, 1960 (DOI: [10.1039/b800140p](#))

**Theoretical evaluation of nano- or microparticulate contact angle at fluid/fluid interfaces: analysis of the excluded area behavior upon compression**

D. O. Grigoriev, H. Möhwald and D. G. Shchukin, *Phys. Chem. Chem. Phys.*, 2008, **10**, 1975 (DOI: [10.1039/b719140e](#))

# Au–Pd supported nanocrystals prepared by a sol immobilisation technique as catalysts for selective chemical synthesis†

Jose Antonio Lopez-Sanchez,<sup>a</sup> Nikolaos Dimitratos,<sup>a</sup> Peter Miedziak,<sup>a</sup> Edwin Ntainjua,<sup>a</sup> Jennifer K. Edwards,<sup>a</sup> David Morgan,<sup>a</sup> Albert F. Carley,<sup>a</sup> Ramchandra Tiruvalam,<sup>b</sup> Christopher J. Kiely<sup>b</sup> and Graham J. Hutchings\*<sup>a</sup>

Received 14th December 2007, Accepted 23rd January 2008

First published as an Advance Article on the web 18th February 2008

DOI: 10.1039/b719345a

Catalysis by gold and gold–palladium nanoparticles has attracted significant research attention in recent years. These nanocrystalline materials have been found to be highly effective for selective and total oxidation, but in most cases the catalysts are prepared using precipitation or impregnation. We report the preparation of Au–Pd nanocrystalline catalysts supported on carbon prepared *via* a sol-immobilisation technique and these have been compared with Au–Pd catalysts prepared *via* impregnation. The catalysts have been evaluated for two selective chemical syntheses, namely, oxidation of benzyl alcohol and the direct synthesis of hydrogen peroxide. The catalysts have been structurally characterised using a combination of scanning transmission electron microscopy and X-ray photoelectron spectroscopy. The catalysts prepared using the sol immobilisation technique show higher activity when compared with catalysts prepared by impregnation as they are more active for both hydrogen peroxide synthesis and hydrogenation, and also for benzyl alcohol oxidation. The method facilitates the use of much lower metal concentrations which is a key feature in catalyst design, particularly for the synthesis of hydrogen peroxide.

## Introduction

At present there is a fascination with the design of nanoparticles and nanostructured materials and developing improved routes for the preparation of these materials is the focus of much current research, particularly for gold nanoparticles.<sup>1</sup> The reason for gold being of particular interest is two-fold. Firstly, from a preparative point of view, gold is the most stable noble metal at the nanoscale and has an extensive surface chemistry. This has provided the impetus to devise improved preparation routes for gold nanoparticles, and there is considerable interest in the fabrication of ligand protected gold nanoparticles.<sup>1–5</sup> Secondly, the recent discovery of the catalytic efficacy of gold nanocrystals for oxidation and reduction reactions has been a major driving force for research into novel catalytic applications of gold nanoparticles. This has enabled a new approach in the search for selective redox catalysts.<sup>6–12</sup> Supported gold catalysts have been shown to be effective for low temperature oxidation of CO,<sup>13</sup> even in the presence of H<sub>2</sub>, H<sub>2</sub>O and CO<sub>2</sub> and this reaction is finding some potential application in fuel cells.<sup>14,15</sup> Gold has also been

found to be effective for the selective oxidation of alkenes<sup>16,17</sup> and alcohols,<sup>18</sup> and for the selective hydrogenation of unsaturated carbonyl compounds and nitro groups.<sup>19</sup>

Although there is a rich catalytic chemistry unfolding for pure gold nanoparticles, we have recently shown that the combination of gold and palladium in an alloy nanoparticle configuration leads to enhanced catalytic activity and selectivity in redox processes. In particular, we have shown that although gold alone is a very effective catalyst for the selective oxidation of an alcohol to an aldehyde under solvent free conditions,<sup>18</sup> the alloying of gold with palladium leads to a twenty five-fold enhancement in activity with simultaneous retention of selectivity.<sup>20</sup> While palladium alone is an exceptionally effective catalyst for the direct hydrogenation of molecular oxygen to produce hydrogen peroxide,<sup>21</sup> the alloying of gold with the palladium significantly enhances the activity and selectivity for this challenging reaction.<sup>22–27</sup> These two specific reactions provide the focus for the present study since they are representative examples of selective oxidation and hydrogenation that are of key importance in selective chemical synthesis.

The oxidation of primary alcohols to aldehydes is an important laboratory and commercial procedure.<sup>28–30</sup> Aldehydes are valuable both as intermediates and as high value components for the perfume industry.<sup>28</sup> Often oxidations of this type are carried out using stoichiometric oxygen donors such as chromate or permanganate, but these reagents are expensive and have serious toxicity and environmental issues associated with them.<sup>28</sup> Given these limitations, there is substantial interest in the development of heterogeneous catalysts that use molecular O<sub>2</sub> as the oxidant. Au nanocrystals have been shown to be highly effective for the oxidation of alcohols

<sup>a</sup> School of Chemistry, Cardiff University, Main Building, Park Place, Cardiff, UK CF10 3AT. E-mail: hutch@cardiff.ac.uk; Fax: +44 29 2087 4059; Tel: +44 29 2087 4059

<sup>b</sup> Center for Advanced Materials and Nanotechnology, Lehigh University, 5 East Packer Avenue, Bethlehem, PA 18015-3195, USA  
† Electronic supplementary information (ESI) available: Bright field micrograph of the sol-immobilized AuPd/C sample after use as a catalyst (Fig. S1); bright field micrograph and corresponding histogram of the particle size distribution of the AuPd/C sol-immobilized sample after calcination at 400 °C (Fig. S2). See DOI: 10.1039/b719345a

with O<sub>2</sub> in an aqueous base, in particular diols and triols; although under these conditions, the product is the corresponding mono-acid, not the aldehyde.<sup>31–33</sup> However, gold in the absence of base has recently been shown to be highly effective for the oxidation of alcohols.<sup>12</sup>

The direct hydrogenation of O<sub>2</sub> to give hydrogen peroxide remains one of the grand challenges in catalytic chemistry. At present this important commodity chemical which is produced on a major scale, *ca.* 2 M tons per annum, is used mainly as a bleach and disinfectant. It is manufactured using an indirect method which is based on the sequential hydrogenation and oxidation of an alkyl anthraquinone,<sup>34</sup> that avoids molecular hydrogen and oxygen coming into direct contact. However, a direct reaction could be preferable to the current indirect process. Indeed, there is a recent report<sup>35</sup> that a direct process using a Pd-based catalyst is being commercialised, which represents a major step forward in the manufacture of this important material. The direct reaction between hydrogen and oxygen has been a research target for many years, with the first reported study in 1914,<sup>36</sup> using a Pd catalyst. Since then, there have been a number of investigations<sup>37–49</sup> emanating mainly from industrial laboratories and until recently all these catalyst design studies have been based on supported palladium catalysts. We have recently shown that the addition of gold to the palladium enhances the formation of hydrogen peroxide in the direct synthesis process.<sup>22–27</sup>

In our previous work, where we demonstrated that the combination of gold and palladium provides a pronounced synergistic effect in redox catalysis,<sup>22–27</sup> we have prepared the catalysts *via* an impregnation procedure in which 5 wt% total metal loading was utilized. It could, however, be economically and practically beneficial to utilise lower concentrations of gold and palladium since this approach may afford improved dispersions of the nanocrystals. In this paper we investigate the use of lower concentrations of these precious metals using a sol-immobilisation method of preparation. We have recently shown that this methodology is effective for the synthesis of monometallic gold and palladium catalysts<sup>50</sup> and we now investigate the applicability of this method for generating gold–palladium alloy nanoparticles supported on carbon.

## Experimental

### Catalyst preparation

The following notation is used for the catalyst samples we have prepared: I denotes impregnation, SI denotes sol-immobilisation, *w* denotes Au and Pd are present as 1 : 1 by weight, and *m* denotes Au and Pd are present as 1 : 1 molar ratio.

**Impregnation method.** 1 wt% Pd-only, 1 wt% Au-only and Au–Pd bimetallic catalysts were prepared by impregnation of carbon (Darco G60, Aldrich), *via* an impregnation method using aqueous solutions of PdCl<sub>2</sub> (Johnson Matthey) and/or HAuCl<sub>4</sub>·3H<sub>2</sub>O (Johnson Matthey). For the 0.5%Au–0.5%Pd/carbon catalyst, the detailed preparation procedure employed is described below. An aqueous solution of HAuCl<sub>4</sub>·3H<sub>2</sub>O (2 ml, 5 g dissolved in water (250 ml)) and an aqueous solution of PdCl<sub>2</sub> (0.83 ml, 1 g in water (25 ml)) were simultaneously added to carbon (3.8 g). The paste formed was ground and

dried at 110 °C for 16 h and calcined in static air, typically at 400 °C for 3 h.

**Sol-immobilisation method.** An aqueous solution of PdCl<sub>2</sub> (Johnson Matthey) and HAuCl<sub>4</sub>·3H<sub>2</sub>O of the desired concentration was prepared. Polyvinylalcohol (PVA) (1 wt% solution, Aldrich, *M<sub>w</sub>* = 10 000, 80% hydrolyzed) was added (PVA/Au (by wt) = 1.2); a 0.1 M freshly prepared solution of NaBH<sub>4</sub> (>96%, Aldrich, NaBH<sub>4</sub>/Au (mol/mol) = 5) was then added to form a dark-brown sol. After 30 min of sol generation, the colloid was immobilized by adding activated carbon (acidified at pH 1 by sulfuric acid) under vigorous stirring conditions. The amount of support material required was calculated so as to have a total final metal loading of 1 wt%. After 2 h the slurry was filtered, the catalyst washed thoroughly with distilled water (neutral mother liquors) and dried at 120 °C overnight. Two catalysts were prepared using a 1 : 1 molar ratio of Au : Pd (denoted Au–Pd/C<sub>SI<sub>m</sub></sub>) and a 1 : 1 weight ratio of Au : Pd (denoted Au–Pd/C<sub>SI<sub>w</sub></sub>). Monometallic catalysts containing gold or palladium were also prepared using similar methodology, and these are denoted Au/C<sub>SI</sub> and Pd/C<sub>SI</sub>.

### Catalyst testing

**Benzyl alcohol oxidation.** The benzyl alcohol oxidation reactions were carried out in a stirred reactor (100 mL, Autoclave Engineers Inline MagneDrive III). The vessel was charged with alcohol (40 mL) and catalyst (0.1 g). The autoclave was then purged 5 times with oxygen leaving the vessel at 10 bar gauge. The stirrer was set at 1500 r.p.m. and the reaction mixture was raised to the required temperature. Samples from the reactor were taken periodically, *via* a sampling system. For the analysis of the products a GC-MS and GC (a Varian star 3400 cx with a 30 m CP-Wax 52 CB column) were employed. The products were identified by comparison with known standards samples. For the quantification of the amounts of reactants consumed and products generated, the external calibration method was used.

**Hydrogen peroxide synthesis and hydrogenation.** Catalyst testing was performed using a stainless steel autoclave (Parr Instruments) with a nominal volume of 50 ml and a maximum working pressure of 14 MPa. The autoclave was equipped with an overhead stirrer (0–2000 rpm) and provision for measurement of temperature and pressure. Typically, the autoclave was charged with the catalyst (0.01 g unless otherwise stated), solvent (5.6 g MeOH and 2.9 g H<sub>2</sub>O), purged three times with 5% H<sub>2</sub>/CO<sub>2</sub> (3 MPa) and then filled with 5% H<sub>2</sub>/CO<sub>2</sub> and 25% O<sub>2</sub>/CO<sub>2</sub> to give a hydrogen to oxygen ratio of 1 : 2 at a total pressure of 3.7 MPa. Stirring (1200 rpm unless otherwise stated) was commenced on reaching the desired temperature (2 °C), and all experiments were carried out for 30 min unless otherwise stated. Gas analysis for H<sub>2</sub> and O<sub>2</sub> was performed by gas chromatography using a thermal conductivity detector and a CP – Carboplot P7 column (25 m, 0.53 mm id). H<sub>2</sub>O<sub>2</sub> yield was determined by titration of aliquots of the final filtered solution with acidified Ce(SO<sub>4</sub>)<sub>2</sub> (7 × 10<sup>–3</sup> mol l<sup>–1</sup>). Ce(SO<sub>4</sub>)<sub>2</sub> solutions were standardised against (NH<sub>4</sub>)<sub>2</sub>Fe(SO<sub>4</sub>)<sub>2</sub>·6H<sub>2</sub>O using ferroin as indicator. Hydrogen peroxide

hydrogenation was carried out in an identical manner but in this case the 25% O<sub>2</sub>/CO<sub>2</sub> was not added so that hydrogen peroxide could not be synthesised, but part of the water was replaced by hydrogen peroxide (50 vol%) to give a hydrogen peroxide concentration of 4 wt%.

### Catalyst characterisation

The sols were characterized using a UV spectrometer (V-570, JASCO) in H<sub>2</sub>O between 200 and 1200 nm, in a quartz cuvette.

Samples for examination by analytical electron microscopy (AEM) were prepared by dispersing the catalyst powder in high purity ethanol, then allowing a drop of the suspension to evaporate on a holey carbon film supported by a 300 mesh copper TEM grid. Samples were then subjected to chemical microanalysis and annular dark-field imaging in a VG Systems HB603 scanning transmission electron microscope (STEM) operating at 300 kV equipped with a Nion C<sub>s</sub> corrector. This instrument was also fitted with an Oxford Instruments INCA TEM 300 system for energy dispersive X-ray (XEDS) analysis. Bright field diffraction contrast imaging experiments were carried out on a JEOL 2000FX TEM operating at 200 kV.

X-Ray photoelectron spectra were recorded on a Kratos Axis Ultra DLD spectrometer employing a monochromatic AlK<sub>α</sub> X-ray source (75–150 W) and analyser pass energies of 160 eV (for survey scans) or 40 eV (for detailed scans). Samples were mounted using a double-sided adhesive tape and binding energies referenced to the C(1s) binding energy of adventitious carbon contamination which was taken to be 284.7 eV.

## Results and discussion

### Preparation and characterisation of the sols and catalysts

**Characterisation of the sols.** UV-Vis spectra (200–900 nm) of the Au and Pd sols were recorded in H<sub>2</sub>O. For the Au sol the plasmon resonance band was located at 505 nm (Fig. 1a). This band is characteristic of the plasmon resonance band of gold nanoparticles having a size of <10 nm.<sup>51,52</sup> In contrast to gold, Pd metallic sols display no surface plasmon band (Fig. 1b);<sup>53</sup> therefore, we observe the disappearance of the precursor peak after reduction ( $\lambda_{\text{max}} = 210$  and 238 nm) as has previously been reported.<sup>51</sup> The spectra resulting from the mixture of the two metal sols indicates the disappearance of the gold surface plasmon band as previously reported for this system.<sup>51</sup> This is a phenomena commonly found in the formation of sols of bimetallic nanoparticles where one of the component metals lacks a surface plasmon band. An example of this phenomena is demonstrated in the formation of Ag–Rh nanoparticles where the effect was attributed to the spontaneous formation of Ag-core/Rh-shell particles.<sup>54</sup> In the particular case of gold and palladium, Deki *et al.*<sup>55</sup> dispersed nanoparticles of several Au–Pd compositions on a polymer thin film matrix and concluded that the progressive decrease of the gold plasmon band in the UV-Vis spectra observed by increasing the palladium content was the result of changes in the band structure of the Au particles due to alloying with Pd. Also the formation of nanocomposites from Au–COO<sup>−</sup> and

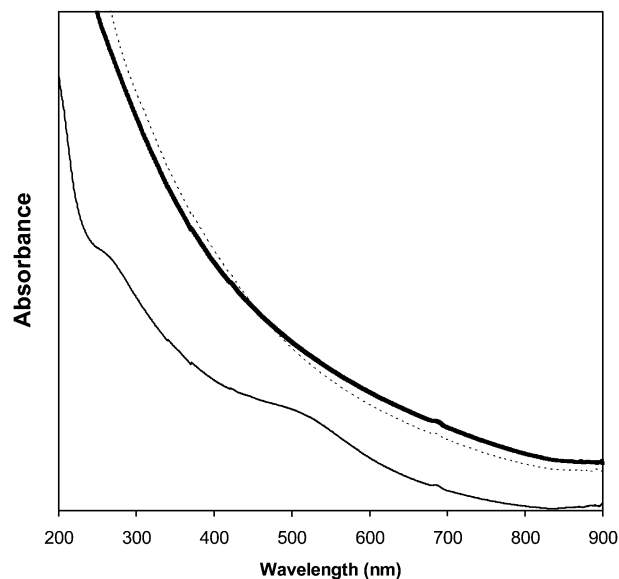


**Fig. 1** UV-Vis spectra of sol-immobilised catalysts. Key: 1 wt% Au/C<sub>Si</sub> (—), 1 wt% Pd/C<sub>Si</sub> (·····) and 1 wt% Au–Pd/C<sub>SiIm</sub> (— · —).

Pd–NH<sub>3</sub><sup>+</sup> resulted in the disappearance of the gold plasmon resonance.<sup>56</sup>

**XPS characterization.** Fig. 2 shows the Au(4f) and Pd(3d) spectra for the dried and calcined 1 wt% AuPd (1 : 1 by wt)/C catalysts, prepared by both sol-immobilisation and impregnation. For all the samples the Au(4f) spectra (Fig. 2a) show no change in the oxidation state, and the binding energy is indicative of the presence of metallic gold. In contrast, the Pd(3d) spectra (Fig. 2b) show significant changes on calcination. The uncalcined samples exhibit predominantly Pd<sup>0</sup> species which on calcination transform to mainly Pd<sup>2+</sup>, but with a small residual Pd<sup>0</sup> component. The dramatic decrease in the Au(4f) and Pd(3d) spectral intensities for the impregnated samples as compared with the sol immobilization prepared samples, as evident in Fig. 2, is reflected in the calculated molar elemental ratios, as discussed later (Table 3). In order to calculate the molar ratios, the Pd(3d) intensity is first corrected for the presence of an overlapping Au(4d<sub>3/2</sub>) component, by subtracting an intensity calculated from that of the well-resolved Au(4d<sub>3/2</sub>) peak.

**Electron microscopy characterization.** The size distribution of the supported metal nanoparticles for both the impregnated and sol-immobilized AuPd/C samples was assessed from analysis of bright field TEM micrographs such as those presented in Fig. 3a and c, respectively. In the sample made *via* the impregnation route, the particle size ranged between 2 and 14 nm, with the average size being around 6 nm (Fig. 3b). Occasional larger particles in excess of 25 nm were also seen in this material, although these were relatively rare. By comparison, the metal particle size distribution in the catalyst prepared by sol-immobilization was found to be much narrower, *i.e.* between 4–7 nm, as shown in Fig. 3d.

The compositions of the metal particles in these two materials were monitored by STEM-XEDS (*i.e.* X-ray energy dispersive analysis) spectrum imaging. A representative annular

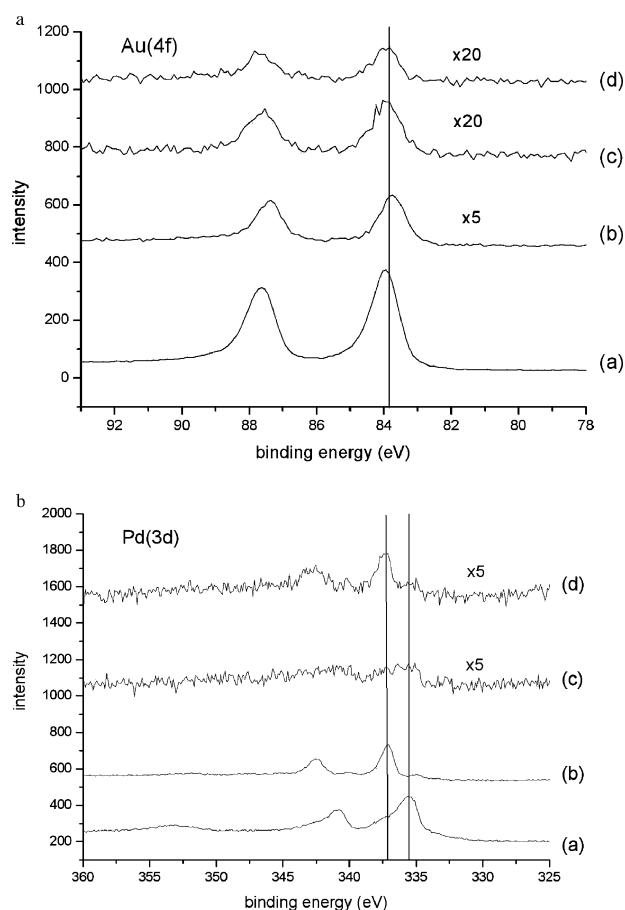


**Fig. 2** Au(4f) spectra (plot a) and Pd(3d) spectra (plot b) for 1 wt% Au–Pd/C catalysts (Au : Pd = 1 : 1 by wt) prepared by sol immobilisation [(a) dried and (b) calcined at 400 °C] and impregnation [(c) dried and (d) calcined at 400 °C].

dark field (ADF) image and the corresponding Au  $L_{\alpha 1}$  and Pd  $L_{\alpha 1}$  elemental maps from the impregnated AuPd/C sample are shown in Fig. 4. It is clear that there is a direct spatial correlation between the Au and Pd signals confirming that all the metal particles are in fact Au–Pd alloys. It is not possible from our present analysis to discern whether the Au–Pd particles are random alloys or core–shell in nature. It is clear however from comparison of the relative Pd and Au signal intensities that the particle compositions within the 4–8 nm size range shown here are all fairly consistent, with the particles being slightly Pd-rich in all cases. This is entirely consistent with previous studies on materials prepared in a similar manner where the AuPd composition as a function of particle size was measured by STEM-XEDS.<sup>57</sup> In this previous work we consistently found that large (~50 nm) particles were Au-rich, intermediate size particles (~15 nm) were closer to the nominal 1 : 1 at% composition, and the very smallest (~5 nm) particles were always Pd-rich. For comparison, a representative ADF image and the corresponding Au  $L_{\alpha 1}$  and Pd  $L_{\alpha 1}$  elemental maps from the area delineated by the box are presented for the sol immobilized AuPd/C samples shown in Fig. 5. The quality of the X-ray mapping data is not as good in this instance because of the significant contamination we

encountered during the experiment due to the degradation of the PVA ligands bound to particle surface under the high fluence of electrons in the incident beam. Even so, we can confirm that the relatively monodisperse particles prepared by the colloidal route are all bimetallic Au–Pd alloys. A significant difference from the impregnated samples, however, can be seen by comparing the relative intensities of the Au  $L_{\alpha 1}$  and Pd  $L_{\alpha 1}$  signals from particle-to-particle. If one compares the neighbouring pairs of particles labelled ‘a’ and ‘b’ or ‘c’ and ‘d’ for instance, it is clear that the composition is quite variable (e.g. particle ‘b’ is considerably more Pd-rich than particle ‘a’). Hence we conclude that even though the colloidal sol-immobilisation route clearly produces a narrower size distribution of particles, the degree of control of particle composition within a particular size interval is not as good as that for the impregnated sample.

### Evaluation of the Au–Pd/C catalysts for selective chemical synthesis

**Benzyl alcohol oxidation.** The oxidation of benzyl alcohol is often used as a model reaction for alcohol oxidation, not only due to its relatively high reactivity but also because of the existence of a complex reaction network (Fig. 6). The target products are benzaldehyde and benzoic acid, but other by-products e.g. toluene, benzene, benzyl benzoate and acetal can form depending on the reaction conditions and metal catalyst employed. These by-products are likely to be the outcome of side reactions due to hydrogenolysis (toluene formation), decarbonylation (benzene) and esterification reaction pathways (benzyl benzoate) (see Fig. 6).

The catalytic data for Au–Pd/C<sub>SI</sub>, Au/C<sub>SI</sub> and Pd/C<sub>SI</sub> are displayed in Fig. 7a and Tables 1 and 2. A comparison between the monometallic catalysts (Au, Pd) supported on carbon indicates that these two catalysts gave very similar activities and selectivities (Table 1). Their selectivities at the same level of conversion (50%) were also found to be similar (Table 2). Comparison at iso-conversion permits a direct and meaningful comparison between the product distributions obtained with each catalyst. The bimetallic Au–Pd/C<sub>SI</sub> catalyst was significantly more active and gave higher yields of benzaldehyde. In particular, the turnover frequency (mol benzyl alcohol oxidized per mol of metal) was markedly higher for the Au–Pd catalyst. However, comparison at iso-conversion (Table 2) showed that the bimetallic catalyst also gave significantly higher yields of toluene formed by hydrogenolysis. It is interesting to compare the activity of the bimetallic catalyst prepared by sol-immobilisation and similar catalysts prepared by impregnation (Fig. 7b and 7c, Tables 1 and 2). It is apparent that the catalysts prepared by the sol immobilisation procedure are more active for benzyl alcohol oxidation to benzaldehyde when compared with catalysts prepared using the impregnation procedure. Analysis by TEM confirmed that the particle size distribution for the Au–Pd/C<sub>SI</sub> sample did not change after reaction (see Fig. S1, ESI).†

In Table 3 we report elemental atomic ratios and total metal loadings derived from XPS analysis of these three samples and also two 1 wt% AuPd/C catalysts prepared by impregnation and corresponding to molar and weight ratios of Au : Pd = 1 : 1. The Pd : Au molar ratio for the bimetallic catalyst

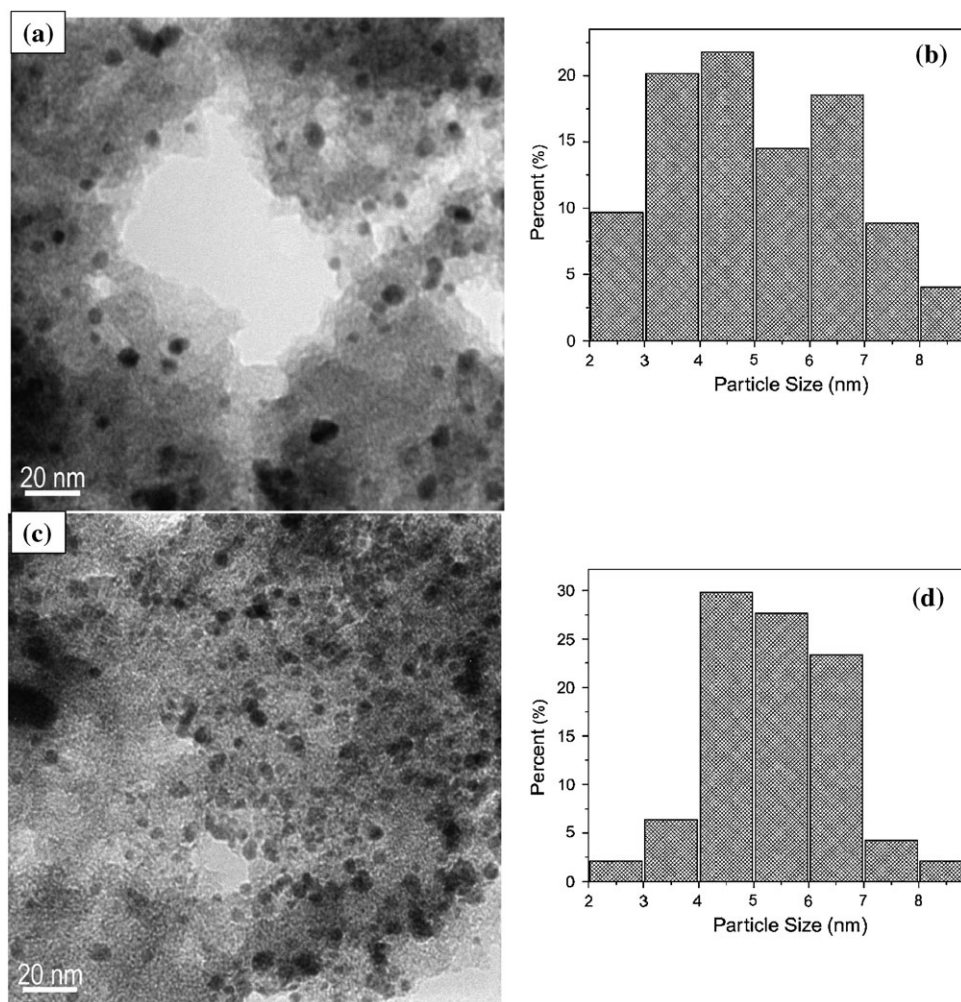


**Fig. 3** Bright field TEM micrographs and the corresponding histograms of the particle size distributions for the AuPd/C samples prepared by impregnation ((a) and (b)) and sol-immobilization ((c) and (d)).

Au–Pd/C<sub>SI</sub>m (0.81) is reasonably close to the expected value of 1.0, indicating that there are few particles present exhibiting the Au-core Pd-shell morphology observed in several other systems involving supported Au–Pd nanoparticles,<sup>22–26</sup> notably oxide supported systems, but this observation is in agreement with our recent observations for carbon-supported Au–Pd nanoparticles prepared by impregnation.<sup>27</sup> Since there is a significant synergistic effect on catalytic activity for the Au–Pd sample compared to the mono-metallic catalysts

(Table 1), a significant fraction of the particles must be present as Au–Pd alloys, and this is in agreement with the observations made by electron microscopy. The impregnated samples show much higher Pd : Au ratios (by a factor > 2) than for the samples prepared by sol immobilization (Table 3), consistent with either the development of Pd-rich shell/Au-rich core particles or a significantly higher Pd dispersion relative to Au compared with the SI catalysts. Elemental analysis of the 1 wt% catalysts prepared by either impregnation or sol-

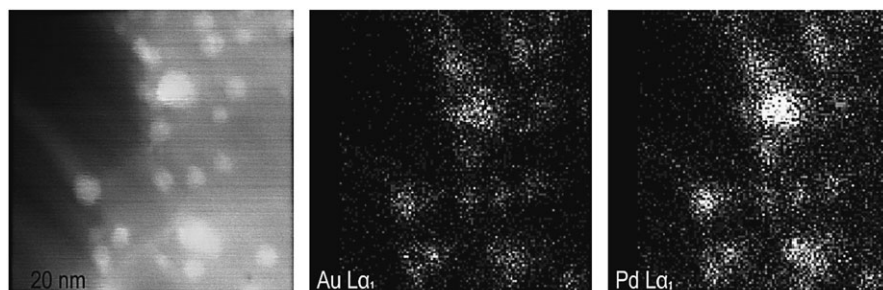


**Fig. 4** STEM–ADF image and the corresponding Au L<sub>α1</sub> and Pd L<sub>α1</sub> elemental maps of the AuPd/C catalyst prepared by the impregnation method.

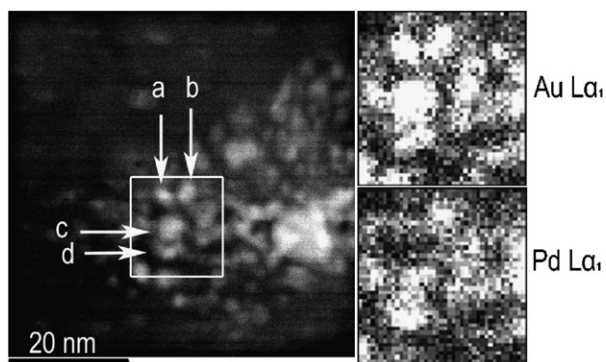


**Fig. 5** STEM-ADF image and the corresponding Au  $L_{\alpha 1}$  and Pd  $L_{\alpha 1}$  elemental maps of the AuPd/C catalyst prepared by the sol-immobilization method.

immobilisation confirms that the metal loading of all the samples is close to the expected nominal value. Although XPS analysis of the impregnated samples also yields metal loadings close to the nominal values (Table 3), extremely high loadings are calculated for the catalysts prepared by sol immobilisation (Table 3). These anomalous values probably arise from the coated metal particles preferentially decorating the exterior surface of the carbon, thereby contributing to the higher catalytic activity we observe, whereas impregnation leads to more effective filling of the pores within the support which in turn means the metal atoms are more homogeneously distributed throughout the material. Since XPS is very surface sensitive the metal signal measured by this technique will

therefore be much higher for the samples prepared by sol-immobilisation. Differences in particle size are not likely to make a large contribution to the differences in apparent metal loading.

AuPd/C<sub>SIW</sub> was also investigated for benzyl alcohol conversion and the results are presented in Fig. 8a. These data show significant differences from those for AuPd/C<sub>SIIm</sub>, AuPd/C<sub>SIW</sub> being much more active and, when the data are compared at iso-conversion it is apparent that the selectivities are very similar (Table 4). We also evaluated Au-Pd/C<sub>Im</sub> at 120 °C which was again found to be less active than Au-Pd/C<sub>SIW</sub> (Fig. 8b) and we observed a TOF of 35 400 h<sup>-1</sup> for AuPd/C<sub>SIW</sub> and 982 for AuPd/C<sub>Im</sub>. The XPS derived Pd : Au molar ratio is 1.47 in this instance as compared with the expected value of 1.86. Both AuPd samples show a somewhat lower Pd content than expected, possibly reflecting a larger average particle size for Pd.

As noted earlier, the catalysts used in our earlier studies<sup>22–27</sup> prepared using impregnation were calcined at 400 °C prior to use. Hence, we have calcined AuPd/C<sub>SIW</sub> and have compared this with catalysts prepared by impregnation, to provide a comparison for the two methods of catalyst synthesis, and the data are shown in Table 1. It is very clear that calcination leads to a decrease in catalyst activity, and the catalyst made by the sol-immobilisation method is more significantly affected by heat treatment. Analysis by TEM of the calcined sample showed that considerable sintering and growth of the Au-Pd nanoparticles has occurred presumably because of disruption of the protective ligand shell at elevated temperatures (see Fig.

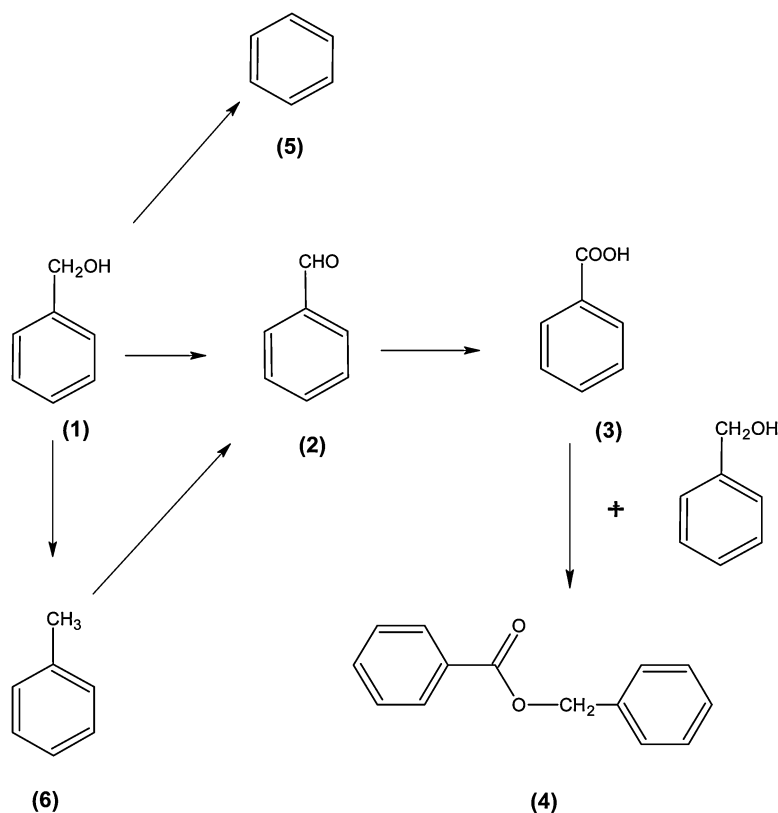


**Fig. 6** General reaction pathway for benzyl alcohol: (1) benzyl alcohol; (2) benzaldehyde; (3) benzoic acid; (4) benzyl benzoate; (5) benzene; (6) toluene.

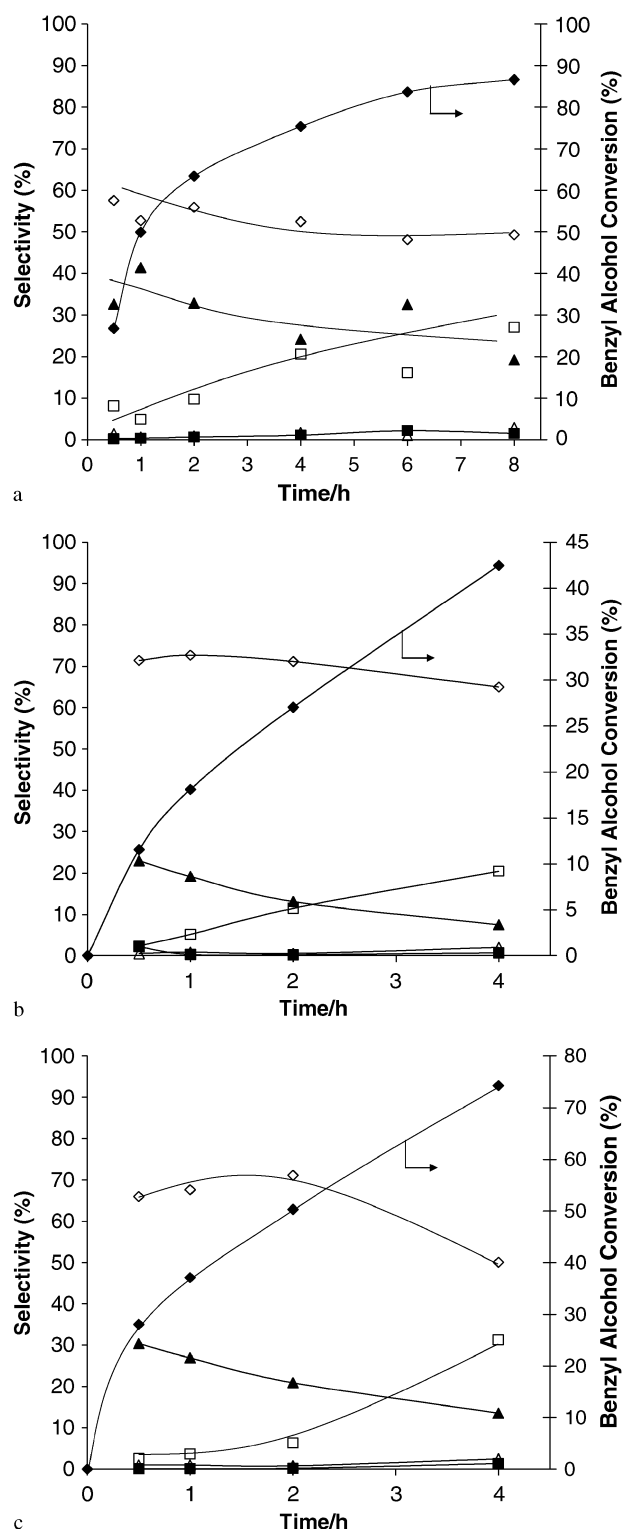


**Fig. 7** Selective oxidation of benzyl alcohol, (a) 1 wt% Au-Pd/C<sub>SI</sub>m; (b) 1 wt% Au-Pd/C<sub>I</sub>m; (c) 1 wt% Au-Pd/C<sub>1w</sub>. Reaction conditions: benzyl alcohol 40 ml, 0.1 g of catalyst,  $T = 160\text{ }^{\circ}\text{C}$ ,  $p\text{O}_2 = 150\text{ psi}$ , time of reaction = 8 h, stirring rate 1500 rpm. Key:  $\blacklozenge$  benzyl alcohol conversion (%),  $\blacksquare$  benzene selectivity (%),  $\blacktriangle$  toluene selectivity (%),  $\diamond$  benzaldehyde selectivity (%),  $\square$  benzoic acid selectivity (%) and  $\triangle$  benzyl benzoate selectivity (%).

S2, ESI).<sup>†</sup> Using TGA we have observed that the PVA is largely lost by oxidation from the catalyst on heating at  $350\text{ }^{\circ}\text{C}$ . Hence, we consider that when we calcine the catalysts at  $400\text{ }^{\circ}\text{C}$  the PVA is largely removed. For the dried materials, at this stage, we do not know how much of the PVA remains on the catalyst after drying and clearly this could play a role in the observed catalysis with the dried materials and we will attempt to address this issue in subsequent studies.

**Hydrogen peroxide synthesis and hydrogenation.** A series of catalysts, prepared either by sol-immobilisation (Au/C<sub>SI</sub>, Pd/C<sub>SI</sub>, AuPd/C<sub>SI</sub>m, AuPd/C<sub>SI</sub>m) or by co-impregnation (AuPd/C<sub>I</sub>m, AuPd/C<sub>1w</sub>) all containing 1 wt% total metal, with carbon as support, were investigated for the direct synthesis of hydrogen peroxide; the results for reaction at  $2\text{ }^{\circ}\text{C}$  are shown in Table 6. For the so-immobilisation set, the pure Au catalyst did generate some H<sub>2</sub>O<sub>2</sub> but at a very low rate, whereas the Pd only catalyst was more active. However, the addition of Au to Pd markedly enhanced the catalyst activity by a factor of 36. This is the most dramatic synergistic effect we have observed to date for the direct synthesis of hydrogen peroxide. Comparison of the Au-Pd catalysts prepared by sol-immobilisation with the corresponding Au-Pd catalysts prepared by impregnation (Table 5) shows that the catalysts prepared by sol-immobilisation are significantly more active. This dramatic enhancement in activity is a feature that we will investigate in greater detail in subsequent studies. One of the key problems with respect to the synthesis of hydrogen peroxide is the stability of the product under reaction conditions where hydrogen peroxide is present with high pressure H<sub>2</sub>. It is generally acknowledged that catalysts that are effective for the synthesis reaction, *e.g.* supported Pd catalysts, are all effective hydrogenation catalysts, since their primary role is the activation of H<sub>2</sub> at low temperatures. This creates a major problem, since catalysts that are effective in the initial hydrogenation of oxygen to give hydrogen peroxide selectively are also equally effective at the hydrogenation of hydrogen peroxide to water in a subsequent hydrogenation reaction (see Fig. 9). We have found that the decomposition of hydrogen peroxide to give oxygen and water is not observed during the direct reaction when hydrogen is present, *i.e.*  $k_4$  is not significant under our reaction conditions,<sup>23,27</sup> and the loss of selectivity we observe is principally due to the hydrogenation of hydrogen peroxide.<sup>27</sup> This is because the selectivity for hydrogen peroxide we observe at very low conversions approaches 100%, indicating that  $k_3$  is not significant. Hence, under our reaction conditions the eventual yield of hydrogen peroxide is governed by the relative ratio of  $k_1$  and  $k_2$ . In view of this we have investigated the hydrogenation of hydrogen peroxide (Table 6) and it is evident that the sol-immobilised catalysts are more active for the sequential hydrogenation of hydrogen peroxide as well as its synthesis (Table 6). Clearly, this is a crucial area of catalyst design that requires further attention if the higher activity of the sol-immobilised catalysts is to be realised for hydrogen peroxide synthesis.

## Conclusions

In our earlier studies based on carbon-supported Au-Pd alloy nanoparticles prepared by impregnation we have shown these

**Table 1** Liquid phase oxidation of benzyl alcohol for catalysts containing 1 wt% of metal prepared by the sol-immobilization and impregnation methods

Catalyst	Conversion %	Selectivity/%			Yield/%			TOF/h <sup>-1</sup> <sup>a</sup>
		Toluene	Benzaldehyde	Benzoic acid	Toluene	Benzaldehyde	Benzoic acid	
1% Au-Pd/C <sub>SI</sub> <sup>b</sup>	82	31.0	48.0	18.0	25.4	39.4	14.8	29 900
1% Au/C <sub>SI</sub> <sup>b</sup>	48	5.8	64.4	22.8	2.8	30.8	10.9	14 800
1% Pd/C <sub>SI</sub> <sup>b</sup>	56	8.2	61.0	23.7	10.9	34.2	13.3	16 200
1% Au-Pd/C <sub>SIw</sub> <sup>c</sup>	81.1	40.9	55.0	1.3	33.17	44.61	1.05	35 404
1% AuPd/C <sub>SIw</sub> <sup>c</sup> treated/400 °C	6.7	2.4	78.7	3.6	0.16	5.27	0.24	1770
1% Au-Pd/C <sub>Im</sub> <sup>b</sup>	44.6	7.5	65.0	20.5	3.2	27.6	8.7	17 265
1% Au-Pd/C <sub>Im</sub> <sup>b</sup> treated/400 °C	72.1	24.0	56.6	15.7	17.3	40.8	11.3	12 656
1% Au-Pd/C <sub>Iw</sub> <sup>b</sup>	74.3	13.5	50.1	31.3	10.0	37.2	23.3	29 914
1% Au-Pd/C <sub>Iw</sub> <sup>b</sup> treated/400 °C	47.8	19.0	73.8	3.1	9.1	35.3	1.5	7154

<sup>a</sup> TOF (h<sup>-1</sup>) at 0.5 h of reaction. TOF numbers were calculated on the basis of total loading of metals. <sup>b</sup> Reaction conditions: benzyl alcohol, catalyst (0.1 g), *T* = 160 °C, pO<sub>2</sub> = 10 bar, time of reaction = 4 h, stirring rate 1500 rpm. <sup>c</sup> Reaction conditions: benzyl alcohol, 0.1 g of catalyst, *T* = 120 °C, time of reaction = 2 h, pO<sub>2</sub> = 150 psi, stirring rate 1500 rpm.

**Table 2** Liquid phase oxidation of benzyl alcohol for catalysts containing 1 wt% total metal loading. Product distribution selectivities were determined at iso-conversion (50%)

Catalyst	S <sub>50</sub> %					
	Benzene	Toluene	Benzaldehyde	Benzoic acid	Benzyl benzoate	Acetal
1% Au-Pd/C <sub>SI</sub>	0.3	41.4	53.0	4.9	0.7	0
1% Au/C <sub>SI</sub>	0.7	5.2	63.5	24.2	6.5	0
1% Pd/C <sub>SI</sub>	1.3	12.6	66.0	16.2	3.9	0
1% Au-Pd/C <sub>Im</sub>	0.9	4.2	61.9	25.0	2.7	0
1% Au-Pd/C <sub>Iw</sub>	0.2	20.9	71.1	6.3	0.8	0

<sup>a</sup> Reaction conditions: benzyl alcohol, 0.1 g of catalyst, *T* = 160 °C, pO<sub>2</sub> = 10 bar, stirring rate 1500 rpm. S<sub>50</sub> indicate the selectivity observed at 50% conversion.

**Table 3** XPS derived elemental atomic ratios for carbon supported AuPd, Au and Pd catalysts prepared by sol-immobilisation. Total metal loading for each sample is 1 wt% and all samples were dried at 120 °C overnight

Sample	Nominal Pd : Au	Elemental ratios and total metal loading derived from XPS peak intensities					
		Pd/Au	Pd/C	Au/C	(Au + Pd)/C	O/C	wt% metal
AuPd/C <sub>SI</sub>	1/1 molar	0.81	0.013	0.017	0.030	0.144	39
Au/C <sub>SI</sub>	0/1			0.027	0.027	0.114	49
Pd/C <sub>SI</sub>	1/0		0.017		0.017	0.139	15
AuPd/C <sub>SIw</sub>	1/1 Weight (1.85:1 molar)	1.47	0.015	0.010	0.024	0.136	29
AuPd/C <sub>I</sub>	1/1 molar	2.37	0.0007	0.0003	0.001	0.00441	1.08
AuPd/C <sub>I</sub>	1/1 Weight (1.85:1 molar)	3.29	0.0011	0.0003	0.0014	0.0485	1.49

**Table 4** Liquid phase oxidation of benzyl alcohol for catalysts prepared by sol-immobilization

Catalyst	Selectivity at 50% conversion/%						TOF/h <sup>-1</sup> <sup>c</sup>
	Benzene	Toluene	Benzaldehyde	Benzoic acid	Benzyl benzoate	Acetal	
1% AuPd/C <sub>SI</sub> <sup>a</sup>	0.3	41.4	52.7	4.9	0.7	0.0	29 900
1% AuPd/C <sub>SIw</sub> <sup>b</sup>	0.3	44.0	51.3	1.7	2.7	0.1	35 400

<sup>a</sup> Reaction conditions: benzyl alcohol, 0.1 g of catalyst, *T* = 160 °C, pO<sub>2</sub> = 150 psi. <sup>b</sup> Reaction conditions: benzyl alcohol, 0.1 g of catalyst, *T* = 120 °C, pO<sub>2</sub> = 150 psi. <sup>c</sup> Calculation of TOF (h<sup>-1</sup>) after 0.5 h of reaction. TOF numbers were calculated on the basis of total loading of metals. S<sub>50</sub> indicate the selectivity observed at 50% conversion.

to be present in a broad particle size range (typically 3–7 nm but with a number of particles > 10 nm).<sup>27,52</sup> We have also shown these materials to exhibit very high activity for both the synthesis of hydrogen peroxide<sup>27</sup> and the oxidation of alcohols

to aldehydes.<sup>20</sup> We used the relatively simple impregnation method during the catalyst discovery phase of these studies precisely because it generates a broad range of potential active species, and hence improves our chances of determining

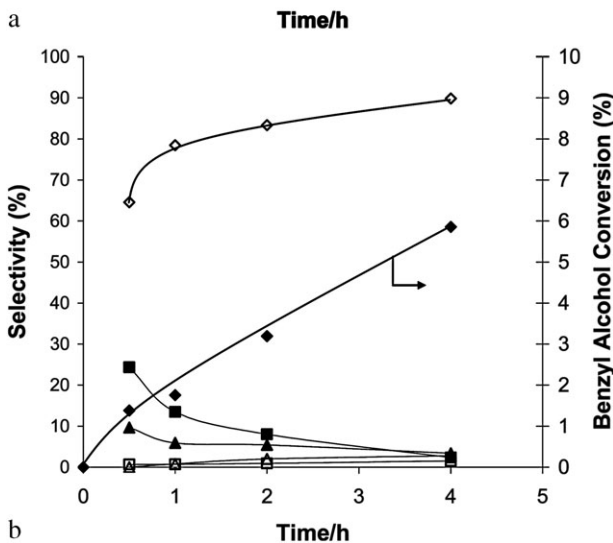
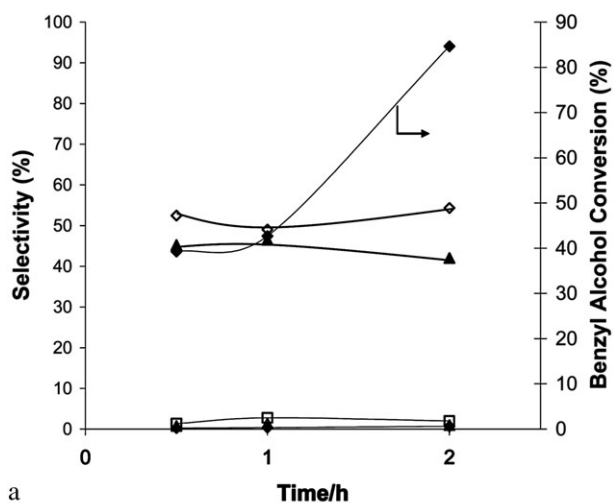


**Fig. 8** Selective oxidation of benzyl alcohol, (a) 1 wt% Au-Pd/C<sub>S1w</sub>; (b) 1 wt% Au-Pd/C<sub>Iw</sub> (reaction conditions: benzyl alcohol 40 ml, 0.1 g of catalyst,  $T = 120\text{ }^{\circ}\text{C}$ ,  $p\text{O}_2 = 150\text{ psi}$ , time of reaction = 2 h, stirring rate 1500 rpm. Key:  $\blacklozenge$  benzyl alcohol conversion (%),  $\blacksquare$  benzene selectivity (%),  $\blacktriangle$  toluene selectivity (%),  $\diamond$  benzaldehyde selectivity (%),  $\square$  benzoic acid selectivity (%),  $\triangle$  benzyl benzoate selectivity (%) and  $\circ$  acetal selectivity (%).

whether or not catalyst activity is enhanced with this methodology. In contrast, the sol-immobilisation method leads to a distinctly narrower particle size range of Au-Pd alloy nano-

**Table 5** Hydrogen peroxide productivity for catalysts prepared by sol-immobilization and impregnation on a carbon support<sup>a</sup>

Catalyst	Hydrogen peroxide productivity	
	Mol H <sub>2</sub> O <sub>2</sub> kg <sup>-1</sup> (cat) h <sup>-1</sup>	Mol H <sub>2</sub> O <sub>2</sub> mol <sup>-1</sup> (metal) h <sup>-1</sup>
1% Au/C <sub>SI</sub>	0.21	4.1
1% Pd/C <sub>SI</sub>	1.51	16.1
1% AuPd/C <sub>SIIm</sub>	54.1	820
1% Au-Pd/C <sub>SIw</sub>	128.0	1775
AuPd/C <sub>Im</sub>	12.0	181
Au-Pd/C <sub>Iw</sub>	60.0	832

<sup>a</sup> Reaction conditions: reaction time for H<sub>2</sub>O<sub>2</sub> synthesis 30 min; Mass of catalyst for H<sub>2</sub>O<sub>2</sub> synthesis: 10 mg, all catalysts uncalcined.

**Table 6** Hydrogen peroxide hydrogenation results for catalysts prepared by sol-immobilization and impregnation on a carbon support<sup>a</sup>

Catalyst	Hydrogen peroxide hydrogenation/%
1% AuPd/C <sub>SIIm</sub>	27
1% Au-Pd/C <sub>SIw</sub>	18
AuPd/C <sub>Im</sub>	4
Au-Pd/C <sub>Iw</sub>	7

<sup>a</sup> Reaction conditions, all catalysts uncalcined. MeOH (5.6 g), H<sub>2</sub>O (2.22 g), H<sub>2</sub>O<sub>2</sub> (0.68 g) and 0.1 g catalyst, 5% H<sub>2</sub>/CO<sub>2</sub>,  $P = 420\text{ psi}$ ,  $T = 2\text{ }^{\circ}\text{C}$ , stirring speed = 1200 rpm and reaction time = 30 min.

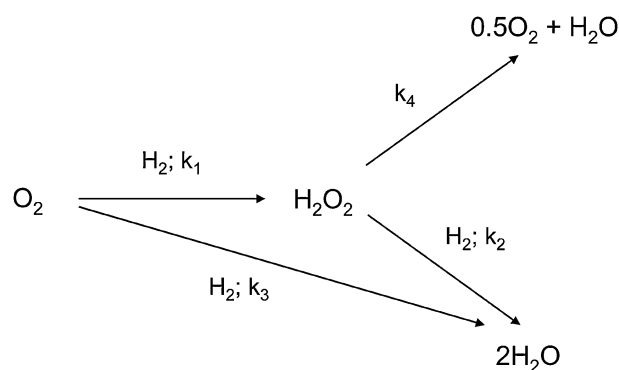


**Fig. 9** Reaction scheme for the synthesis of hydrogen peroxide from the reaction of O<sub>2</sub> and H<sub>2</sub>.

particles. However, both methods lead to the formation of alloy nanoparticles and X-ray photoelectron spectroscopy together with STEM-XDS show that in both cases the particles are homogeneous alloys. The sol-immobilised catalysts display different activities when compared with the materials prepared by impregnation, being more active for hydrogen peroxide synthesis and also for alcohol oxidation. The sol-immobilisation method certainly permits a greater control of the particle size distribution design parameter, but controlling the compositional homogeneity as a function of particle size still needs some further development. Studies have shown that Au-Pd alloy nanoparticles are of interest for the formation of vinyl acetate<sup>58</sup> and the cyclisation of acetylene<sup>59</sup> and hence the results of this study may have general applicability.

## Acknowledgements

This work formed part of the EU AURICAT project (Contract HPRN-CT-2002-00174) and the EPSRC/Johnson Matthey funded ATHENA project and we thank them for funding this research. We also thank the World Gold Council (through the GROW scheme), and Cardiff University (AA Reed studentship) for providing support for J.K.E. C.J.K. and R.T. would also like to acknowledge the financial support of the NSF Nanomanufacturing program under contract #CMMI-0457602).

## References

- J. Shan and H. Tenhu, *Chem. Commun.*, 2007, 4580.

- 2 M.-C. Daniel and D. Astrue, *Chem. Rev.*, 2004, **104**, 293.
- 3 L. M. Liz-Mnazarán, *Mater. Today*, 2004, **7**, 26.
- 4 J. Turkevich, P. C. Stevenson and J. Hillier, *Discuss. Faraday Soc.*, 1951, **11**, 55.
- 5 M. Brust, M. Walker, D. Bethell, D. J. Schiffrin and C. J. Kiely, *J. Chem. Soc., Chem. Commun.*, 1994, 801.
- 6 G. C. Bond and D. T. Thompson, *Catal. Rev. Sci. Eng.*, 1999, **41**, 319.
- 7 G. C. Bond and D. T. Thompson, *Gold Bull.*, 2000, **33**, 41.
- 8 M. Haruta, *Gold Bull.*, 2004, **37**, 27.
- 9 A. S. K. Hashmi, *Gold Bull.*, 2004, **37**, 51.
- 10 R. Meyer, C. Lemaire, Sh. K. Shaikudinov and H.-J. Freund, *Gold Bull.*, 2004, **37**, 72.
- 11 G. J. Hutchings, *Gold Bull.*, 2004, **37**, 37.
- 12 A. S. K. Hashmi and G. J. Hutchings, *Angew. Chem., Int. Ed.*, 2006, **45**, 7896.
- 13 M. Haruta, T. Kobayashi, H. Sano and N. Yamada, *Chem. Lett.*, 1987, **16**, 405.
- 14 P. Landon, J. Ferguson, B. E. Solsona, T. Garcia, A. F. Carley, A. A. Herzing, C. J. Kiely, S. E. Golunski and G. J. Hutchings, *Chem. Commun.*, 2005, 3385.
- 15 P. Landon, J. Ferguson, B. E. Solsona, T. Garcia, S. Al-Sayari, A. F. Carley, A. Herzing, C. J. Kiely, M. Makkee, J. A. Moulijn, A. Overweg, S. E. Golunski and G. J. Hutchings, *J. Mater. Chem.*, 2006, **16**, 199.
- 16 A. K. Sinha, S. Seelan, S. Tsubota and M. Haruta, *Angew. Chem., Int. Ed.*, 2004, **43**, 1546.
- 17 M. D. Hughes, Y.-J. Xu, P. Jenkins, P. McMorn, P. Landon, D. I. Enache, A. F. Carley, G. A. Attard, G. J. Hutchings, F. King, E. H. Stitt, P. Johnston, K. Griffin and C. J. Kiely, *Nature*, 2005, **437**, 1132.
- 18 A. Abad, P. Conception, A. Corma and H. Garcia, *Angew. Chem., Int. Ed.*, 2005, **44**, 4066.
- 19 A. Corma and P. Serna, *Science*, 2006, **313**, 332.
- 20 D. I. Enache, J. K. Edwards, P. Landon, B. Solsona-Espriu, A. F. Carley, A. A. Herzing, M. Watanabe, C. J. Kiely, D. W. Knight and G. J. Hutchings, *Science*, 2006, **311**, 362.
- 21 V. R. Choudhary and C. Samanta, *J. Catal.*, 2006, **238**, 28.
- 22 P. Landon, P. J. Collier, A. J. Papworth, C. J. Kiely and G. J. Hutchings, *Chem. Commun.*, 2002, 2058.
- 23 P. Landon, P. J. Collier, A. F. Carley, D. Chadwick, A. J. Papworth, A. Burrows, C. J. Kiely and G. J. Hutchings, *Phys. Chem. Chem. Phys.*, 2003, **5**, 1917.
- 24 B. E. Solsona, J. K. Edwards, P. Landon, A. F. Carley, A. Herzing, C. J. Kiely and G. J. Hutchings, *Chem. Mater.*, 2006, **18**, 2689.
- 25 J. K. Edwards, B. Solsona, P. Landon, A. F. Carley, A. Herzing, M. Watanabe, C. J. Kiely and G. J. Hutchings, *J. Mater. Chem.*, 2005, **15**, 4595.
- 26 J. K. Edwards, B. E. Solsona, P. Landon, A. F. Carley, A. Herzing, C. J. Kiely and G. J. Hutchings, *J. Catal.*, 2005, **236**, 69.
- 27 J. K. Edwards, A. F. Carley, A. A. Herzing, C. J. Kiely and G. J. Hutchings, *Faraday Discuss.*, 2008, in press.
- 28 R. A. Sheldon and J. K. Kochi, *Metal-Catalyzed Oxidations of Organic Compounds*, Academic Press, New York, 1981.
- 29 G. ten Brink, I. W. C. E. Arends and R. A. Sheldon, *Science*, 2000, **287**, 1636.
- 30 M. Pagliaro, S. Campestrini and R. Ciriminna, *Chem. Soc. Rev.*, 2005, **34**, 837.
- 31 L. Prati and M. Rossi, *J. Catal.*, 1998, **176**, 552.
- 32 F. Porta, L. Prati, M. Rossi and G. Scari, *J. Catal.*, 2002, **211**, 464.
- 33 F. Porta and L. Prati, *J. Catal.*, 2004, **224**, 397.
- 34 H. T. Hess, in *Kirk-Othmer Encyclopaedia of Chemical Engineering*, ed. I. Kroschwitz and M. Howe-Grant, Wiley, New York, 1995, vol. 13, p. 961.
- 35 'Degussa Headwaters builds peroxide demonstrator', *The Chemical Engineer*, 2005, **766**, p. 16.
- 36 H. Henkel and W. Weber, US Pat., 1108752, 1914.
- 37 G. A. Cook, US Pat., 2368640, 1945.
- 38 Y. Izumi, H. Miyazaki and S. Kawahara, US Pat., 4009252, 1977.
- 39 Y. Izumi, H. Miyazaki and S. Kawahara, US Pat., 4279883, 1981.
- 40 H. Sun, J. J. Leonard and H. Shalit, US Pat., 4393038, 1981.
- 41 L. W. Gosser and J.-A. T. Schwartz, US Pat., 4772458, 1988.
- 42 L. W. Gosser, US Pat., 4889705, 1989.
- 43 C. Pralins and J.-P. Schirmann, US Pat., 4996039, 1991.
- 44 T. Kanada, K. Nagai and T. Nawata, US Pat., 5104635, 1992.
- 45 J. Van Weynbergh, J.-P. Schoebrechts and J.-C. Colery, US Pat., 5447706, 1995.
- 46 S.-E. Park, J. W. Yoo, W. J. Lee, J.-S. Chang, U. K. Park and C. W. Lee, US Pat., 5972305, 1999.
- 47 G. Paparatto, R. d'Aloisio, G. De Alberti, P. Furlan, V. Arca, R. Buzzoni and L. Meda, EP Pat., 0978316A1, 1999.
- 48 B. Zhou and L.-K. Lee, US Pat., 6168775, 2001.
- 49 M. Nystrom, J. Wangard and W. Herrmann, US Pat., 6210651, 2001.
- 50 N. Dimitratos, J. A. Lopez-Sanchez, D. Morgan, A. Carley, L. Prati and G. J. Hutchings, *Catal. Today*, 2007, **122**, 317.
- 51 C. L. Bianchi, P. Canton, N. Dimitratos, F. Porta and L. Prati, *Catal. Today*, 2005, **102**, 203.
- 52 S. Link and M. A. El-Sayed, *J. Phys. Chem. B*, 1999, **103**, 4212.
- 53 J. A. Creighton and D. G. Eadon, *J. Chem. Soc., Faraday Trans.*, 1991, **87**, 3881.
- 54 K. Hirakawa and N. Toshima, *Chem. Lett.*, 2003, **32**, 78.
- 55 S. Deki, K. Akamatsu, Y. Hatakenaka, M. Mizuhata and A. Kajinami, *Nanostructured Mater.*, 1999, **11**, 59.
- 56 X. Wang, K. Naka, M. Zhu, H. Itoh and Y. Chujo, *Langmuir*, 2005, **21**, 12395.
- 57 A. A. Herzing, M. Watanabe, C. J. Kiely, J. Edwards, M. Conte, Z. R. Tang and G. J. Hutchings, *Faraday Discuss.*, 2008, in press.
- 58 M. Chen, D. Kumar, C.-W. Yi and D. W. Goodman, *Science*, 2005, **310**, 291.
- 59 A. F. Lee, C. J. Baddeley, C. Hardacre, R. M. Ormerod, R. M. Lambert, G. Schmid and H. West, *J. Phys. Chem.*, 1995, **99**, 6096.